

# Tracking Chirality in Photoelectron Circular Dichroism

Marek W. Heger and Daniel M. Reich

*Dahlem Center for Complex Quantum Systems and Fachbereich Physik,  
Freie Universität Berlin, Arnimallee 14, D-14195 Berlin, Germany*

(Dated: May 24, 2024)

Photoelectron circular dichroism (PECD) originates from the interplay between a molecule's chiral nuclear scaffold and a circularly polarized ionizing laser field. It is one of the most sensitive characterization techniques for the chirality of molecules in the gas phase. However, due to the complexity of the observable, it is generally difficult to predict and track how and when the chirality of the molecule is imprinted onto the photoelectron. Here, we present simulations of PECD for single-photon ionization in a hydrogenic single-electron model with an artificial chiral potential. This framework allows us to systematically tune the system's chirality and characterize the emergence of PECD. To this end, we propose chirality measures for potentials and wave functions to establish a quantitative connection with the resulting anisotropy in the photoelectron distribution. We show that these chirality measures are suitable indicators for chirality in our model, paving the way for tracking the evolution of chirality from the nuclear scaffold to the final observable.

Chiral molecules play an important role in biology, chemistry, and physics [1–4] since their handedness prominently affects interactions with chiral light and matter. A chiral molecular scaffold gives rise to a chiral potential and imprints a notion of handedness on the system which can be probed and measured via suitable observables. Prominent examples for such observables are microwave three-wave mixing [5–12], circular dichroism (CD) [13–18], and photoelectron circular dichroism (PECD) [19–27], with the latter allowing for anisotropies of around 10% in many molecular species. While it has been shown that PECD in the gas phase is strongly driven by short-range interactions [28], it was recently demonstrated that even in a hydrogen atom, excitations to chiral intermediate states lead to a PECD signal after interaction with circularly polarized light despite the absence of a chiral short range potential [29]. This highlights the complex interplay of the nuclear geometry, the initial electronic wave function, and the interaction with the circularly polarized driving field. In general, the initial state inherits its chirality from the nuclear scaffold, which underlines the role of geometric properties of the system in generating chiral signatures. Candidates for geometric measures of quantifying chirality were previously investigated in several studies [29–32]. They have been formulated for, e.g., electron densities, point mass distributions, photoelectron distributions as well as electric fields, however, a comprehensive discussion of chirality measures for potentials and wave functions has so far been missing. In this work, we propose a chirality measure for potentials and wave functions. We analyse its ability to track the emergence of PECD as one of the paradigmatic chiral observables and investigate in how far such a measure can be used to predict the strength of PECD. To keep the chiral system in our study as simple and tuneable as possible, we consider single photon ionization of hydrogen subject to an artificial chiral potential which mimics the local chiral environment of elec-

trons in PECD experiments. We present time-dependent simulations of the electron dynamics in this model systems which demonstrate a qualitative and quantitative link between the anisotropy in the photoelectron distribution and our chirality measures for the potential and the electronic wave function at final time.

The starting point for our model is the Hamiltonian

$$H(t) = H_{\text{H}} + gV_{\text{chiral}} + \mathbf{A}(t) \cdot \mathbf{p}, \quad (1)$$

with  $H_{\text{H}}$  the Hamiltonian for atomic hydrogen,  $\hat{V}_{\text{chiral}}$  an artificial chiral potential with a scaling factor  $g$ , and  $\mathbf{A}(t) \cdot \mathbf{p}$  the interaction with a laser field in the electric dipole approximation using velocity gauge. The chiral potential  $\hat{V}_{\text{chiral}}$  introduces chirality to the system. We expand it in real-valued spherical harmonics  $Y_{lm}$ , i.e.,

$$V_{\text{chiral}} = V(r) \sum_{lm} c_{lm} Y_{lm}(\varphi, \theta), \quad (2)$$

with expansion coefficients  $c_{lm}$ . This toy model allows us to systematically tune the system's chirality. Our study is focused on the angular dependence which plays the critical role in breaking inversion symmetry. To this end, we treat the radial dependence  $V(r)$  as a simple prefactor for the spherical harmonic expansion, thus limiting any chirality to emerge from the chiral potential via the  $c_{lm}$ . By tuning these coefficients, the chirality of the system can be directly controlled. For the radial shape  $V(r)$  we employ a screened Coulomb potential with a screening length of 4 Bohr, localizing the effect of the potential around the chiral center. This screening together with the hydrogenic nature of our system is reminiscent of tightly-bound K shell electron in a chiral molecules chiral center, although the details of the potential will be more complex in a proper molecular environment.

We systematically study the dependence of the chirality of  $V_{\text{chiral}}$  on the coefficients  $c_{lm}$  by truncating the expansion in Eq. (2) at different values of  $L$ . A restriction

to low values of  $L$  allows us to construct chiral potentials via a simple spherical harmonics expansion featuring only few coefficients. A similar low-order expansion for states has been applied to study propensity rules in PECD in Ref. [33]. Although in realistic chiral molecules much higher orders in  $L$  will commonly be involved [34], electromagnetic potentials with low  $L$  can be artificially engineered via generating low-order multipole moments using static electric fields [35]. When imprinting chirality in such an external fashion, one could mimic random orientations of molecules in the gas phase by rotating the fields with respect to the ionizing pulse. Note, however, that the radial dependence of the potential in such a framework would differ from the screened Coulomb profile in our model.

In photoelectronic circular dichroism the system's chirality is probed via ionization using a circularly polarized light field, cf. the final term in Eq. (1). This leads to a forwards-backwards asymmetry of photoelectrons even for randomly oriented molecular targets. For simplicity, we restrict ourselves to single-photon ionization in this study. To simulate the PECD in our toy model we solve the time-dependent Schrödinger equations (TDSE) utilizing the Runge-Kutta propagator. We represent the angular degree of freedom of the electronic wave function via spherical harmonics and the radial degree of freedom via a Gauss-Lobatto Finite Element Discrete Variable Representation [36, 37]. The photoelectron spectra are continuously extracted during time evolution using the time-dependent surface flux method (t-SURFF) [38, 39]. Furthermore, we employ a complex absorbing potential (CAP) [40] to avoid unphysical reflections.

To simulate PECD in the gas phase we need to account for arbitrary orientations of the chiral potential with respect to the propagation direction of the laser field. To this end, we calculate the photoelectron spectra of multiple individual orientations  $P^{\alpha\beta\gamma}$  obtained by rotating  $V_{\text{chiral}}$  via the Euler angles  $\alpha\beta\gamma$ . Since every orientation requires a full propagation of the laser-induced dynamics, we use the efficient Lebedev scheme [41] to keep the numerical effort low.

For the quantification of chirality of the potential and the wave functions in our setup we introduce a chirality measure inspired by Refs. [29–32]. The precise definition of such a measure needs to be chosen carefully such that the key property is ensured: achiral objects need to be mapped to a value of zero, chiral objects should be mapped to a nonzero value. To this end, we need to distinguish the quantification of chirality for potentials and wave functions. For the case of potentials - or, more generally, real-valued scalar functions  $f(\mathbf{r})$  - we define

$$\chi^V(f(\mathbf{r})) = \frac{\min_{\alpha\beta\gamma} \int_{\mathbb{R}^3} |R^{\alpha\beta\gamma} P f^c(\mathbf{r}) - f^c(\mathbf{r})|^2 d^3r}{4 \int_{\mathbb{R}^3} |f(\mathbf{r})|^2 d^3r}. \quad (3)$$

The idea of Eq. (3) is to find the minimal overlap between  $f^c(\mathbf{r})$  and its mirror image  $P f^c(\mathbf{r})$  via arbitrary rotations

$R^{\alpha\beta\gamma}$  in a proper frame of reference. To perform the rotations in such a frame we define  $f^c(\mathbf{r}) = T f(\mathbf{r})$  with  $T$  a translation such that the first moment of  $f^c(\mathbf{r})^2$  is zero.

Before we explain the importance of choosing the frame of reference via the first moment, we emphasize that Eq. (3) cannot be used as a chirality measure for wave functions. This is because states which differ only by a global phase would not be treated equivalently by the above definition. To amend this, we represent the state as a density matrix to ensure that any global phase has no impact on the chirality measure,

$$\chi^\rho(\rho) = \frac{\min_{\alpha\beta\gamma} \|R^{\alpha\beta\gamma} P \rho^c P^\dagger R^{\alpha\beta\gamma\dagger} - \rho^c\|_{\text{HS}}^2}{2\|\rho\|_{\text{HS}}^2}. \quad (4)$$

Here,  $\|\cdot\|_{\text{HS}}$  is the Hilbert-Schmidt norm and, analogously to Eq. (3),  $\rho^c$  is obtained from the density matrix  $\rho$  via a translation to a frame in which the first moment, i.e. the position expectation value, is zero. As mentioned previously, it is critical to evaluate the minimization over all rotations in a suitable frame of reference. This is because a chirality measure which only minimizes over all rotations in an arbitrary frame can lead to achiral objects being assigned a non-zero value. As pointed out in Ref. [30], one can avoid this issue altogether by performing a minimization over all translations on top of the rotations, however, the practical evaluation of this minimization is highly demanding. As mentioned in Ref. [32], an alternative approach is to evaluate the measures with minimization only over rotations in a coordinate system where the first moment, i.e. the ‘‘center of mass’’, of  $f(\mathbf{r})^2$ , respectively  $\rho(\mathbf{r})$ , vanishes. We could indeed prove (see Supplementary Material) that in such a frame of reference the chirality measures from Eqs. (3) and (4) are guaranteed to yield  $\chi = 0$  for achiral objects even when only minimizing over the set of rotations. This also ensures that chiral objects are guaranteed to yield nonzero chirality measure. Moreover, the resulting value of  $\chi$  will be an upper bound to a chirality measure which includes minimization over both rotations and translations. Finally, we want to highlight that the above measures are scalar - not pseudoscalar - quantities. This avoids the occurrence of chiral zeros [42]. However, this comes at the cost of not being able to characterize the handedness of an object, since, e.g., two enantiomeric forms of a chiral object would be mapped to the same value by our measures.

For our PECD simulations we employ optimized angular chiral potentials obtained by truncating the spherical harmonics expansion at order  $L$  and treating the radial part as a perfectly localized  $\delta$ -function. We performed numerical optimizations with the Nelder-Mead simplex methods to obtain coefficients  $c_{lm}$  with maximize the value of  $\chi^V$  from Eq. (2). The potentials we obtained are visualized in Fig. 1 together with the corresponding optimized value for the chirality measures we obtained

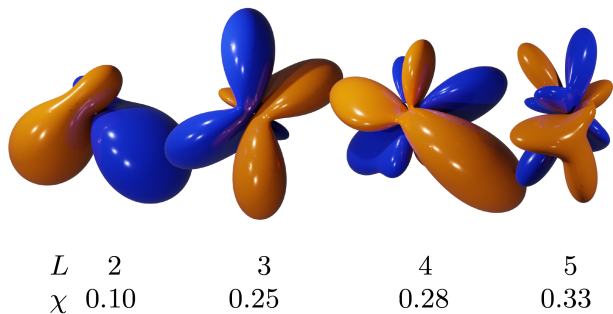


FIG. 1. Isosurfaces with values  $-0.3$  (blue) and  $0.3$  (orange) for chiral potentials according to Eq. (2) with optimized coefficients  $c_{lm}$  for angular expansions up to  $L = 2 - 5$  and  $g = 1$ . The value of the chirality measure according to Eq. (3) is indicated below each potential.

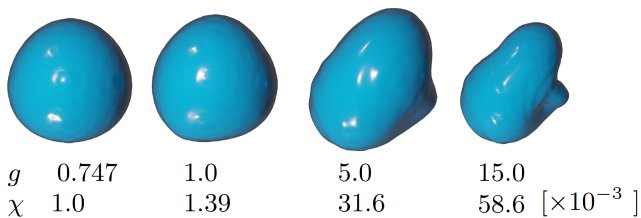


FIG. 2. Isosurfaces with value  $0.03$  of ground-state electron density obtained for the optimized  $L = 3$  chiral potential and different strengths  $g$  of the chiral potential. The value of the chirality measure according to Eq. (4) is shown below each state.

(more details in the Supplementary Material). We observe that for larger truncation limit  $L$ , the values of  $\chi^V$  which can be reached increase as well, with a particularly noticeable jump from  $L = 2$  to  $L = 3$ . This jump is not surprising since a larger value of  $L$  allows for more parameters and thus degrees of freedom which can be explored during the optimization. Note that for  $L \geq 3$  we expect our solutions to only be local extrema. Finding the global maxima for arbitrary  $L$  and taking into account the radial part of the potential will be subject of future work.

The potential imprints chirality onto the electron, which is often prominently reflected in the ground state wave function  $|\psi_0\rangle$ . The connection between potential and ground state is particularly direct for small chiral strengths  $g$  where the chiral potential can be considered as a perturbation to the achiral  $H_H$ , cf. Eq. (1). In leading-order perturbation theory this leads to a chirality measure of the ground state  $\chi(|\psi_0\rangle)$  which is proportional to  $g^2$ . In this perturbative region, we observe that increasing  $g$  thus directly translates to scaling the chirality of the system. Fig. 2 visualizes the gradual deformation of the ground-state electron density for the  $L = 3$  chiral potential for increasing  $g$  and illustrates how the chirality measure for states from Eq. (4) captures this increase in

chirality. For small  $g$  the ground state is predominantly of  $s$ -type, with increasing contributions from  $p$  and  $d$  orbitals for larger values of  $g$ . For large values of  $g$  the electron density increasingly follows the attractive (blue) part of the chiral potential, cf. Fig. 1. For all calculations throughout this work we ensured to remain in the regime where the chiral potential can be seen as a perturbation. This is a realistic assumption for, e.g., the local chiral potentials of K-shell electrons in chiral molecules which served as the inspiration for our toy model.

We furthermore employed our chirality measure to track the dynamic evolution of chirality in our system. To this end, we average the chirality measure for the electronic wave function over all orientations in our simulations. We call the rotationally averaged chirality measure  $\bar{\chi}$ . Fig. 3 shows  $\bar{\chi}$  for the time-dependent wave function using the  $L = 3$  chiral potential with  $g = 0.747$  (cf. Fig. 1). The ionizing pulse is circularly polarized with a length of  $2.41$  fs, a wavelength of  $45.5$  nm, and a sine-squared temporal envelope. The time-dependent cartesian components of the pulse in the polarization plane are shown in the lower panel and the total ionization yield is shown in the upper panel, reaching a value of  $13\%$  by the end of the pulse. The  $1-\sigma$  standard deviation for  $\bar{\chi}$  over all orientation is shown in the upper panel by the orange-shaded area. Note that the orientationally averaged chirality measures are identical for both enantiomers in our simulation due to the fact that the measures from Eqs. (3) and (4) do not distinguish left-handed from right-handed orientations.

We find that the chirality measure of the time-dependent wave function steadily increases during the ionization process and reaches a value larger than the chirality measure of the ground state for all orientations. The orientationally averaged value  $\bar{\chi}$  is given by around  $10^{-3}$  at  $t = 0$  and steadily increases during ionization by almost a factor of two. These trends persists for all potentials in Fig. 1 in the perturbative regime (data not shown).

Finally, we investigated whether chirality of the ground state and of the electronic wave function can be related to the strength of the chiral observable, i.e., the PECD signal. The PECD signal can be characterized by expanding the orientationally averaged photoelectron angular distribution via Legendre coefficients  $c_i$ . The sum of the odd-order Legendre coefficients quantifies the asymmetry of the photoelectron angular distribution which gives rise to the so-called linear PECD (LPECD)[43],

$$\text{LPECD} = \frac{1}{c_0} \left( 2c_1 - \frac{1}{2}c_3 + \frac{1}{4}c_5 - \frac{5}{32}c_7 + \dots \right), \quad (5)$$

with  $c_0$  the total ionization signal. While the coefficients in Eq. (5) are generally energy-dependent, for the single-photon ionization we studied in this work we can average their values around the ionization peak. Note that to ensure a fair comparison we tuned the pulse frequency in

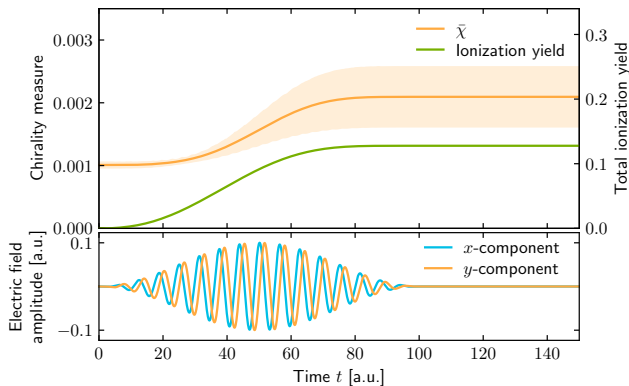


FIG. 3. (Top) Orientationally averaged chirality measure of the time-evolved state for the optimized  $L = 3$  potential with  $g = 0.747$ . The average chirality measure for the left handed potential (blue) overlaps exactly with their right-handed counterpart (blue). The light-orange shaded area shows the  $1\text{-}\sigma$  deviation among all orientations. (Bottom) Electric field components of the circularly polarized pulse in the polarization plane.

all our simulations such that the photoelectron peak position in the spectrum stayed consistently at 0.5 Hartree for all chiral potentials we employed. Moreover, to separate the emergence of chirality in the ionization process from the chirality in the initial ground state, we adjusted the strength of the chiral potential  $g$  in all simulations such that the chirality measure of the ground state is kept at a constant value of  $10^{-3}$ . Concretely, this required  $g$  to be slightly increased for potentials with higher  $L$  cutoff. We attribute this to the fact that higher-order spherical harmonics which are responsible for the coupling to eigenstates of the unperturbed hydrogenic Hamiltonian with higher  $l$  have an diminished influence on the ground state due to the larger energetic distance from the ground state. This leads to a reduced imprint of the chiral potential onto the ground state for these higher-order terms.

Fig. 4 shows the average chirality measure of the wave function at final time  $\bar{\chi}(\psi(T))$ , the chirality measure of the potential  $\chi^V$ , and the value of the resulting LPECD in our simulations. Strikingly, Fig. 4 demonstrates that all chiral quantities move in tandem with increasing  $L$ . This is a strong indicator for the predictiveness of our chirality measures for the potential and the final state in terms of the experimentally observable chiral signature.

Nevertheless, we expect that this predictiveness will have some limits, particularly concerning the assessment of chirality in the electronic continuum. For example, in our model, the chiral potential acts only perturbatively on a ground-state with  $s$ -type character. Thus, in a single-photon ionization process, the most important part of the continuum are  $p$  states. If a chiral potential has large coefficients for  $l = 1$  this can then potentially lead to a higher "effective" chirality which is not distin-

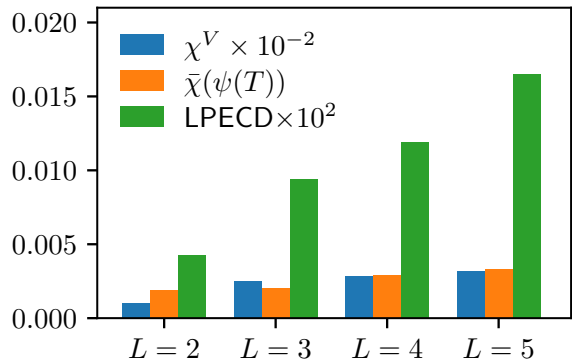


FIG. 4. Chirality measure for potential, wave function at final time, and LPECD for optimized potentials with different value of  $L$ , cf. Fig. 1. The potential scaling factor  $g$  is chosen such that  $\chi(\psi(0)) = 10^{-3}$  throughout.

guished from other contributions by our chirality measure. Moreover, we also evaluated the chirality measure in our simulations for only the continuum, i.e. ionized, part of the time-dependent electronic wave function and observed a steady decrease in its value with time towards an asymptotic value. This curious behavior is likely connected to the propagation of the electron in the chiral potential and the fact that the center of mass of the photoelectron shifts appreciably over time. Although we calculate the chirality measures with respect to this center of mass, we do not minimize over all translations leading to an overestimation of  $\bar{\chi}$ . Nevertheless, we still found that the asymptotic value of the orientationally averaged chirality measure of the continuum part of the wave function is consistently larger than the chirality measure of the ground state, just like it is the case for the total wave function as shown in Fig. 3. Thus, we conjecture that optimal predictiveness of our chirality measure can only be achieved by explicitly accounting for a minimization over translations, too. Further development of the chirality measure in this direction will be subject to future work.

In conclusion, we have shown in a simple model that chirality measures for potentials and wave functions can be used as a tool to track the emergence and predict the strength of chiral observables, such as PECD. Specifically, a large chirality measure of the potential directly translates into a large chirality measure for the ground states and eventually a large PECD signal in our simulations. We emphasize that chirality measures need to be adapted to the physical quantity to be assessed, e.g., by accounting for the physical equivalence of wave functions with respect to a global phase. Moreover, to guarantee that achiral objects are assigned a chirality measure of zero it is important to account for all rotations *and* translations or at least to move to a proper frame of ref-

erence. Although no measure of chirality can be expected to be a perfect quantitative predictor for arbitrary chiral observables, the performance of our chirality measures in the examples we studied here is encouraging in terms of their potential applicability in a wider range of systems and for other chiral observables like, e.g., circular dichroism.

We would like to thank Christiane Koch, Raoul Ebeling, Alexander Blech, and Bar Ezra for helpful discussions. Financial support by the Deutsche Forschungsgemeinschaft (DFG, German Research Foundation)—Projektnummer 328961117—SFB ELCH 1319 is gratefully acknowledged.

## SUPPLEMENTARY MATERIAL

In the following we provide further details on the properties of the chirality measure discussed in the main text. In particular, we expand on the role of translations, discuss how to account for them, and provide numerical guidance to evaluate the chirality measure in a single-center expansion. Finally, we provide the coefficients for the optimized chiral potentials we employed in our simulations.

### Properties of Chirality Measures

A completely faithful chirality measure for a real-valued function  $f(\mathbf{r})$  with  $\int_{\mathbb{R}^3} |f(\mathbf{r})|^2 d^3r = 1$ , needs to account for minimization over all possible translations  $T_{xyz}$  in addition to rotations. This is because an object is only chiral, if it cannot be superimposed via *translations and rotations* with its mirror image. For quantifying chirality of such scalar functions the corresponding chirality measure reads as follows,

$$\begin{aligned} \chi^V(f(\mathbf{r})) &= \frac{1}{4} \min_{\substack{\alpha\beta\gamma \\ xyz}} \int_{\mathbb{R}^3} |T^{xyz} R^{\alpha\beta\gamma} P f(\mathbf{r}) - f(\mathbf{r})|^2 d^3r \\ &= \frac{1}{2} - \frac{1}{2} \max_{\substack{\alpha\beta\gamma \\ xyz}} \int_{\mathbb{R}^3} f(\mathbf{r}) T^{xyz} R^{\alpha\beta\gamma} P f(\mathbf{r}) d^3r, \end{aligned} \quad (6)$$

where  $\alpha, \beta, \gamma$  are the Euler angles for the rotation operator  $R^{\alpha\beta\gamma}$ , and  $P$  is the operator of spatial inversion. The second line in Eq. (6) is obtained by expanding the  $L^2$  norm and using the fact that all involved operators are unitary.

For quantifying chirality of a state we need to account for the irrelevance of the global phase and obtain the following, similar expression. For simplicity we assume that  $\rho = |\psi\rangle\langle\psi|$  is a pure state with  $\langle\psi|\psi\rangle = 1$ . A generaliza-

tion to mixed states is straightforward.

$$\begin{aligned} \chi^\rho(\rho) &= \frac{1}{2} \min_{\substack{\alpha\beta\gamma \\ xyz}} \|T^{xyz} R^{\alpha\beta\gamma} P \rho P^\dagger R^{\alpha\beta\gamma\dagger} T^{xyz\dagger} - \rho\|_{\text{HS}}^2 \\ &= 1 - \max_{\substack{\alpha\beta\gamma \\ xyz}} |\langle\psi| T^{xyz} R^{\alpha\beta\gamma} P |\psi\rangle|^2. \end{aligned} \quad (7)$$

Note that any global phase obtained by applying  $T^{xyz} R^{\alpha\beta\gamma} P$  to  $|\psi\rangle$  is absorbed due to the modulus. We normalized our measures such that they take values between 0 and 1.

While Eqs. (6) and (7) are very faithful to the geometric nature of chirality, determining the extrema over all  $\alpha\beta\gamma, xyz$  is often numerically unfeasible. For both potentials and states we use in our hydrogenic model a single-center expansion, thus rotations can be realized via Wigner D-matrices and are comparatively simple to perform. Conversely, translations in a single-center expansion create slowly converging sums over an infinite range of partial waves  $l$ .

Neglecting the minimization over translations will always overestimate the chirality measures from Eqs. (6) and (7) since in this case the minimal value is only searched over a subset of parameters. While obtaining an upper bound for  $\chi$  is in itself quite useful, it is in our opinion critical to not lose fundamental properties of the chirality measure, namely (i) achiral objects always yield  $\chi = 0$  and (ii) chiral objects always yield  $\chi > 0$ . Although the latter requirement is still fulfilled even if translations are neglected, the former condition does not hold in general in this case. To exemplify this, consider an arbitrary achiral and localized object in three-dimensional space very far away from the origin. The mirrored object is then also very far away from the origin, but in opposite direction. If translations are not considered, then the chirality measure seeks the optimal match of the object with its mirror image by rotation only. However, the mirror image has to first be brought spatially close to the original object to obtain any overlap in the first place, which reduces the three degrees of freedom for the rotation to one. This is generally insufficient to map all achiral objects to  $\chi = 0$ .

### Adjusting the Frame of Reference

To solve the issue in the example explained above, we show that by adjusting the frame of reference it can be guaranteed that  $\chi = 0$  is obtained for achiral objects even when minimization only occurs over rotations. The proof proceeds as follows: We begin by assuming  $f(\mathbf{r})$  to be achiral. This means, that there exists a solution with  $\alpha_s \beta_s \gamma_s, x_s y_s z_s$  such that

$$f(\mathbf{r}) = T^{x_s y_s z_s} R^{\alpha_s \beta_s \gamma_s} P f(\mathbf{r}). \quad (8)$$

For any arbitrary functional  $G[f(\mathbf{r})]$  the relation

$$G[f(\mathbf{r})] - G[T^{x_s y_s z_s} R^{\alpha_s \beta_s \gamma_s} P f(\mathbf{r})] = 0 \quad (9)$$

must hold. From here we chose

$$G[f(\mathbf{r})] = \int_{\mathbb{R}^3} \mathbf{r} |f(\mathbf{r})|^2 d^3r. \quad (10)$$

Equation (9) allows us to draw the following conclusion: Since  $f(\mathbf{r})^2$  is normalized and qualifies as a density we can identify Eq. (10) as the first moment of  $f(\mathbf{r})^2$ . If this first moment coincides with the origin, then rotations and reflections leave its value invariant. In this case, Eq. (9) can only be valid if the translation operator is the identity. In the chirality measure for states the first moment refers to

$$G[|\psi\rangle] = \langle \psi | \mathbf{r} | \psi \rangle, \quad (11)$$

with  $\mathbf{r}$  the position operator. This shows that in a coordinate system where the first moment is at the origin no translations are required to obtain  $\chi = 0$  for achiral objects. The proof for the chirality measure for states proceeds analogously. Due to the significantly reduced complexity of evaluating the minimum only over rotations without needing to account for translations, we decided to employ these simplified chirality measures throughout the main text.

#### Evaluation of $\chi$ for Shifted Functions in Single-Center Expansions

To evaluate the simplified chirality measures from the main text, a single translation, i.e. a shift of the coordinate system, still needs to be performed. This needs to be carefully addressed in a single-center expansion. We propose to calculate  $\chi$  in momentum space where rotations retain their numerical complexity. This is because positions and momenta behave equivalently under rotations. Conversely, translations become phases in momentum space due to the momentum operator being the generator of translations which is diagonal in momentum space. Equation (6), and analogously Eq. (7), highlight that the greatest degree of numerical complexity lies in the evaluation of  $\langle \psi | T^{xyz} R^{\alpha\beta\gamma} P | \psi \rangle$ . As discussed before, we simplify our chirality measure by considering  $\langle \bar{\psi} | R^{\alpha\beta\gamma} P | \bar{\psi} \rangle$  instead, where  $|\bar{\psi}\rangle = T^{\mathbf{a}} |\psi\rangle$  with  $T^{\mathbf{a}}$  is a translation to a coordinate system where the first moment is at the origin. We focus our discussion on the chirality measure for states in the following, the case for po-

entials proceeds analogously. First, we write our states in the following basis,

$$\phi_{klm}(\mathbf{r}) = f_k(r) Y_l^m(\Omega_r), \quad (12)$$

with radial basis functions  $f_k(r)$  and (complex-valued) spherical harmonics  $Y_l^m(\Omega_r)$ . The Fourier transform to momentum domain then reads,

$$\begin{aligned} \phi_{klm}(\mathbf{p}) &= \frac{1}{\sqrt{2\pi^3}} \iiint e^{-i\mathbf{p}\cdot\mathbf{r}} \phi_{klm}(\mathbf{r}) d\mathbf{r} \\ &= \sqrt{\frac{2}{\pi}} \iiint \sum_{LM} (-i)^L j_L(pr) Y_L^M(\Omega_p) Y_L^{M*}(\Omega_r) \\ &\quad \times Y_l^m(\Omega_r) f_k(r) r^2 \sin\theta dr d\theta d\phi \\ &= \sqrt{\frac{2}{\pi}} (-i)^l Y_l^m(\Omega_p) \cdot g_l^k(p), \end{aligned} \quad (13)$$

with

$$g_l^k(p) = \int j_L(pr) f_k(r) r^2 dr \quad (14)$$

and

$$e^{-i\mathbf{p}\cdot\mathbf{r}} = 4\pi \sum_l \sum_m (-i)^l j_l(pr) Y_l^m(\Omega_p) Y_l^{m*}(\Omega_r). \quad (15)$$

Here,  $j_l$  denotes the spherical bessel function of first kind and  $\Omega = (\theta, \phi)$  are the spherical angles.  $|\psi\rangle$  can then be expanded via coefficients  $c_{klm}$ , i.e.,

$$|\psi(\mathbf{p})\rangle = \sum_{klm} c_{klm} \phi_{klm}(\mathbf{p}). \quad (16)$$

The overlap integral from the chirality measure can then be expressed as

$$\begin{aligned} \langle \bar{\psi} | R^{\alpha\beta\gamma} P | \bar{\psi} \rangle &= \langle T^{\mathbf{a}} \psi(\mathbf{p}) | R^{\alpha\beta\gamma} P | T^{\mathbf{a}} \psi(\mathbf{p}) \rangle \\ &= \langle \psi(\mathbf{p}) | e^{-i\mathbf{a}\cdot\mathbf{p}} R^{\alpha\beta\gamma} P e^{i\mathbf{a}\cdot\mathbf{p}} | \psi(\mathbf{p}) \rangle \\ &= \langle \psi(\mathbf{p}) | e^{-i\mathbf{a}\cdot R^{\alpha\beta\gamma \dagger} \mathbf{p} - i\mathbf{a}\cdot\mathbf{p}} | \psi(-R^{\alpha\beta\gamma \dagger} \mathbf{p}) \rangle \\ &= \langle \psi(\mathbf{p}) | e^{-i\mathbf{p}\cdot R^{\alpha\beta\gamma} \mathbf{a} - i\mathbf{p}\cdot\mathbf{a}} R^{\alpha\beta\gamma} P | \psi(\mathbf{p}) \rangle. \end{aligned} \quad (17)$$

In the following we use the abbreviation  $\mathbf{b} = R^{\alpha\beta\gamma} \mathbf{a} - \mathbf{a}$ . Substituting Eq. (13) and Eq. (16) and employing another plane wave expansion (cf. Eq. (15)) leads to

$c_{lm}$	l	1					2					3					4								
	m	-1	0	1	-2	-1	0	1	2	-3	-2	-1	0	1	2	3	-4	-3	-2	-1	0	1	2	3	4
L	$\chi$																								
2	0.10	$\sqrt{0.5}$	$\frac{3}{5}\sqrt{0.5}$				$\frac{4}{5}\sqrt{0.5}$																		
3	0.25	0.5	-0.5					$\sqrt{\frac{1}{8}}$		$\sqrt{\frac{3}{8}}$															
4	0.28	0.402	-0.488	-0.189				-0.489	0.190			0.149		-0.128		-0.119			0.485						
5	0.33	0.283	0.505				-0.336					0.471		0.338											
6	0.35	0.242	0.540				0.187					-0.444		-0.108											

$c_{lm}$	l	5										6																	
	m	-5	-4	-3	-2	-1	0	1	2	3	4	5	-6	-5	-4	-3	-2	-1	0	1	2	3	4	5	6				
L	$\chi$																												
5	0.33	0.406	0.167		0.154																								
6	0.35	-0.458	-0.216		-0.275										-0.103		-0.499												

TABLE I. Coefficients  $c_{lm}$  obtained from optimization towards maximizing chirality with respect to the chirality measure from the main text. Note that all entries which are not explicitly shown correspond to a value of zero.

$$\begin{aligned}
\langle \bar{\psi} | R^{\alpha\beta\gamma} P | \bar{\psi} \rangle &= 8 \sum_{l,l_1,l_2,k_1,k_2} \sum_{m,m_1,m_2} c_{k_1,l_1,m_1}^* c_{k_2,l_2,m_2} (-i)^{l_2-l_1+l} Y_l^{m*}(\Omega_b) \times \\
&\quad \int Y_{l_1}^{m_1*}(\Omega_p) Y_l^m(\Omega_p) R^{\alpha\beta\gamma} P Y_{l_2}^{m_2}(\Omega_p) \sin \theta d\Omega_p \int g_{l_1}^{k_1}(p)^* g_{l_2}^{k_2}(p) j_l(bp) p^2 dp \\
&= 8 \sum_{l,l_1,l_2,k_1,k_2} \sum_{m_1,m_2} c_{k_1,l_1,m_1}^* c_{k_2,l_2,m_2} A_{m_1,m_2}^{l,l_1,l_2} R_{k_1,k_2}^{l,l_1,l_2}, \tag{18}
\end{aligned}$$

with

$$R_{k_1,k_2}^{l,l_1,l_2} = (-i)^{l_2-l_1+l} \int g_{l_1}^{k_1}(p)^* g_{l_2}^{k_2}(p) j_l(bp) p^2 dp \tag{19}$$

and

$$\begin{aligned}
A_{m_1,m_2}^{l,l_1,l_2} &= \sum_m Y_l^{m*}(\Omega_b) \int Y_{l_1}^{m_1*}(\Omega_p) Y_l^m(\Omega_p) R^{\alpha\beta\gamma} P Y_{l_2}^{m_2}(\Omega_p) \sin \theta d\Omega_p \\
&= (-1)^{l_2-m_1} \sum_M [D_{m_2 M}^{l_2} (R)]^* \sqrt{\frac{(2l_1+1)(2l_2+1)(2l+1)}{4\pi}} \begin{pmatrix} l_1 & l_2 & l \\ 0 & 0 & 0 \end{pmatrix} \\
&\quad \times \begin{pmatrix} l_1 & l_2 & l \\ m_1 & M & -(m_1+M) \end{pmatrix} \left( Y_l^{-(m_1+M)}(\Omega_b) \right)^*. \tag{20}
\end{aligned}$$

Here,  $\begin{pmatrix} \cdot & \cdot & \cdot \\ \cdot & \cdot & \cdot \\ \cdot & \cdot & \cdot \end{pmatrix}$  are the Wigner 3j-symbols and  $D_{mm'}^l$  Wigner D-matrices. The calculation of Eq. (20) can be performed as described above, however, evaluating

Eq. (19) is not quite as straightforward. A suitable approach is to substitute Eq. (14) and to switch the order of integration between  $p$  and  $r$ . This allows to evaluate the integrals over three spherical bessel functions analytically [44]. They are given by

$$\begin{aligned}
i^{l_2-l_1+l} \begin{pmatrix} l_1 & l_2 & l \\ 0 & 0 & 0 \end{pmatrix} \int j_{l_1}(rp) j_{l_2}(r'p) j_l(bp) p^2 dp &= \frac{(-1)^{l_1-l} \pi \beta(\Delta)}{4b} \sqrt{2l+1} \left(\frac{r}{b}\right)^l \left(\frac{r'}{r}\right)^L \sqrt{\binom{2L}{2l}} (2L+1) \times \\
&\quad \begin{pmatrix} l_1 & l-L & L' \\ 0 & 0 & 0 \end{pmatrix} \begin{pmatrix} l_2 & L & L' \\ 0 & 0 & 0 \end{pmatrix} \left\{ \begin{matrix} l_1 & l_2 & L \\ L & l-L & L' \end{matrix} \right\} P_{L'}(\Delta). \tag{21}
\end{aligned}$$

$P_L(x)$  are the legendre polynomials of order  $L$ ,  $\Delta = (r^2 + r'^2 + b^2)/(2rr')$ ,  $\beta(\Delta) = \theta(1-\Delta)\theta(1+\Delta)$  with  $\theta$  the Heavyside function in half-maximum convention and  $\left\{ \begin{matrix} \cdot & \cdot & \cdot \\ \cdot & \cdot & \cdot \end{matrix} \right\}$  denotes the Wigner 6j-symbols.

### Optimized Chiral Potentials

In Table I we report the coefficients  $c_{lm}$  we obtained via numerical maximization of the value of our chirality measure among the set of real-valued functions of the form,

$$f(\mathbf{r}) = \sum_{l=0}^L \sum_{m=-l}^l c_{lm} Y_{lm}(\Omega_r) \delta(r-1), \quad (22)$$

where  $Y_{lm}$  are real-valued spherical harmonics and the expansion is truncated at order  $L$ . We focussed on only optimizing the angular part and thus fixed the radial dependence of  $f(\mathbf{r})$  to a  $\delta$ -function. This leads to the function  $f(\mathbf{r})$  only taking nonzero values on the surface of a sphere centered around the origin. Note that the radius of the sphere, chosen to be equal to one in Eq. (22), does not affect the results. In particular, any non-zero translation of the mirror image always yields a vanishing overlap with the original object. For this reason, optimizing the chirality measure for Eq. (22) with respect to rotations only, i.e., neglecting translations, will perfectly reproduce the value of the completely faithful chirality measure from Eq. (6).

- 
- [1] T. C. Johnstone and S. J. Lippard, The chiral potential of phenanthriplatin and its influence on guanine binding, *J. Am. Chem. Soc.* **136**, 2126 (2014).
- [2] A. Comby, S. Beaulieu, M. Boggio-Pasqua, D. Descamps, F. L egar e, L. Nahon, S. Petit, B. Pons, B. Fabre, Y. Mairesse, and V. Blanchet, Relaxation dynamics in photoexcited chiral molecules studied by time-resolved photoelectron circular dichroism: Toward chiral femtochemistry, *J. Phys. Chem. Lett.* **7**, 4514 (2016).
- [3] I. Deveson, B. Madala, J. Blackburn, C. Barker, T. Wong, K. Barton, M. Smith, D. N. Watkins, and T. Mercer, Chiral dna sequences as commutable controls for clinical genomics, *Nature Communications* **10**, 1342 (2019).
- [4] M. H. M. Janssen and I. Powis, Detecting chirality in molecules by imaging photoelectron circular dichroism, *Phys. Chem. Chem. Phys.* **16**, 856 (2014).
- [5] M. Leibscher, J. Kalveram, and C. P. Koch, Rational pulse design for enantiomer-selective microwave three-wave mixing, *Symmetry* **14**, 10.3390/sym14050871 (2022).
- [6] W. Sun and M. Schnell, Microwave three-wave mixing spectroscopy of chiral molecules in weakly bound complexes, *J. Phys. Chem. Lett.* **14**, 7389 (2023).
- [7] D. Patterson, M. Schnell, and J. M. Doyle, Enantiomer-specific detection of chiral molecules via microwave spectroscopy, *Nature* **497**, 475 (2013).
- [8] V. A. Shubert, D. Schmitz, D. Patterson, J. M. Doyle, and M. Schnell, Identifying enantiomers in mixtures of chiral molecules with broadband microwave spectroscopy, *Angew. Chem. Int. Ed.* **53**, 1152 (2014).
- [9] S. Lobsiger, C. Perez, L. Evangelisti, K. K. Lehmann, and B. H. Pate, Molecular structure and chirality detection by fourier transform microwave spectroscopy, *J. Phys. Chem. Lett.* **6**, 196 (2015).
- [10] J. Lee, J. Bischoff, A. O. Hernandez-Castillo, B. Sartakov, G. Meijer, and S. Eibenberger-Arias, Quantitative study of enantiomer-specific state transfer, *Phys. Rev. Lett.* **128**, 173001 (2022).
- [11] H. Singh, F. E. L. Bergg otz, W. Sun, and M. Schnell, Chiral control of gas-phase molecules using microwave pulses, *Angew. Chem. Int. Ed.* **62**, e202219045 (2023).
- [12] S. R. Domingos, C. P erez, M. D. Marshall, H. O. Leung, and M. Schnell, Assessing the performance of rotational spectroscopy in chiral analysis, *Chem. Sci.* **11**, 10863 (2020).
- [13] C. Log e and U. Boesl, Multiphoton ionization and circular dichroism: New experimental approach and application to natural products, *ChemPhysChem* **12**, 1940 (2011).
- [14] M. Stener, D. D. Tommaso, G. Fronzoni, P. Decleva, and I. Powis, Theoretical study on the circular dichroism in core and valence photoelectron angular distributions of camphor enantiomers., *J. Chem. Phys.* **124** **2**, 10.1063/1.2150438 (2006).
- [15] A. Rizzo, N. Lin, and K. Ruud, Ab initio study of the one- and two-photon circular dichroism of r-(+)-3-methylcyclopentanone, *J. Chem. Phys.* **128**, 164312 (2008).
- [16] F. Pulm, J. Schramm, J. Hormes, S. Grimme, and S. D. Peyerimhoff, Theoretical and experimental investigations of the electronic circular dichroism and absorption spectra of bicyclic ketones, *Chem. Phys.* **224**, 143 (1997).
- [17] A. Bornschlegl, C. Log e, and U. Boesl, Investigation of cd effects in the multi photon ionisation of r-(+)-3-methylcyclopentanone, *Chem. Phys. Lett.* **447**, 187 (2007).
- [18] N. Berova, K. Nakanishi, and R. W. Woody, Circular dichroism: Principles and applications, (2000).
- [19] I. Powis, Photoelectron circular dichroism in chiral molecules, in *Adv. Chem. Phys.* (John Wiley and Sons, Ltd, 2008) Chap. 5, pp. 267–329.
- [20] C. Lux, M. Wollenhaupt, T. Bolze, Q. Liang, J. K ohler, C. Sarpe, and T. Baumert, Circular dichroism in the photoelectron angular distributions of camphor and fenchone from multiphoton ionization with femtosecond laser pulses, *Angew. Chem. Int. Ed.* **51**, 5001 (2012).
- [21] A. Kastner, C. Lux, T. Ring, S. Z ullighoven, C. Sarpe, A. Senftleben, and T. Baumert, Enantiomeric excess sensitivity to below one percent by using femtosecond photoelectron circular dichroism, *ChemPhysChem* **17**, 1119 (2016).
- [22] R. Cireasa, A. E. Boguslavskiy, B. Pons, M. C. H. Wong, D. Descamps, S. Petit, H., Ruf, N. Thir e, A. Ferr e, J. Su arez, J. Higu et, B. E. Schmidt, A. F. Alharbi, F. L egar e, V. Blanchet, B. Fabre, S. Patchkovskii, O. A. Smirnova, Y. Mairesse, and V. R. Bhardwaj, Probing molecular chirality on sub-femtosecond time-scale supplementary material, *Nat. Phys.* **11**, 10.1038/nphys3369

- (2015).
- [23] D. Faccialà, M. Devetta, S. Beauvarlet, N. Besley, F. Calegari, C. Callegari, D. Catone, E. Cinquanta, A. G. Ciriolo, L. Colaizzi, M. Coreno, G. Crippa, G. De Ninno, M. Di Fraia, M. Galli, G. A. Garcia, Y. Mairesse, M. Negro, O. Plekan, P. Prasanna Geetha, K. C. Prince, A. Pusala, S. Stagira, S. Turchini, K. Ueda, D. You, N. Zema, V. Blanchet, L. Nahon, I. Powis, and C. Vozzi, Time-resolved chiral x-ray photoelectron spectroscopy with transiently enhanced atomic site selectivity: A free-electron laser investigation of electronically excited fen-chone enantiomers, *Phys. Rev. X* **13**, 011044 (2023).
- [24] A. Kastner, T. Ring, B. C. Krüger, G. B. Park, T. Schäfer, A. Senftleben, and T. Baumert, Intermediate state dependence of the photoelectron circular dichroism of fen-chone observed via femtosecond resonance-enhanced multi-photon ionization, *J. Chem. Phys.* **147**, 013926 (2017).
- [25] S. Beaulieu, A. Comby, D. Descamps, B. Fabre, G. A. Garcia, R. Géneaux, A. G. Harvey, F. Légaré, Z. Mašín, L. Nahon, A. F. Ordonez, S. Petit, B. Pons, Y. Mairesse, O. Smirnova, and V. Blanchet, Photoexcitation circular dichroism in chiral molecules, *Nat. Phys.* **14**, 484 (2018).
- [26] S. T. Ranecky, G. B. Park, P. C. Samartzis, I. C. Giannakidis, D. Schwarzer, A. Senftleben, T. Baumert, and T. Schäfer, Detecting chirality in mixtures using nanosecond photoelectron circular dichroism, *Phys. Chem. Chem. Phys.* **24**, 2758 (2022).
- [27] A. Comby, D. Descamps, S. Petit, E. Valzer, M. Wloch, L. Pouységu, S. Quideau, J. Bocková, C. Meinert, V. Blanchet, B. Fabre, and Y. Mairesse, Fast and precise chiroptical spectroscopy by photoelectron elliptical dichroism, *Phys. Chem. Chem. Phys.* **25**, 16246 (2023).
- [28] A. N. Artemyev, E. Kutscher, and P. V. Demekhin, Photoelectron circular dichroism of a model chiral anion, *J. Chem. Phys.* **156**, 031101 (2022).
- [29] N. Mayer, S. Patchkovskii, F. Morales, M. Ivanov, and O. Smirnova, Imprinting chirality on atoms using synthetic chiral light fields, *Phys. Rev. Lett.* **129**, 243201 (2022).
- [30] G. Gilat, Chiral coefficient—a measure of the amount of structural chirality, *J. Phys. A* **22**, L545 (1989).
- [31] O. Neufeld, M. Even Tzur, and O. Cohen, Degree of chirality of electromagnetic fields and maximally chiral light, *Phys. Rev. A* **101**, 053831 (2020).
- [32] E. Abraham and A. Nitzan, Molecular chirality quantification: Tools and benchmarks, *J. Chem. Phys.* **160**, 164104 (2024).
- [33] A. F. Ordonez and O. Smirnova, Propensity rules in photoelectron circular dichroism in chiral molecules. i. chiral hydrogen, *Phys. Rev. A* **99**, 043416 (2019).
- [34] E. Kutscher, A. N. Artemyev, and P. V. Demekhin, Photoelectron circular dichroism in fen-chone by short coherent broadband laser pulses, *Phys. Rev. A* **107**, 013107 (2023).
- [35] G. Higgins, C. Zhang, F. Pokorny, H. Parke, E. Jansson, S. Salim, and M. Hennrich, Observation of second- and higher-order electric quadrupole interactions with an atomic ion, *Phys. Rev. Res.* **3**, L032032 (2021).
- [36] K. Balzer, S. Bauch, and M. Bonitz, Efficient grid-based method in nonequilibrium green’s function calculations: Application to model atoms and molecules, *Phys. Rev. A* **81**, 022510 (2010).
- [37] T. N. Rescigno and C. W. McCurdy, Numerical grid methods for quantum-mechanical scattering problems, *Phys. Rev. A* **62**, 032706 (2000).
- [38] A. Scrinzi, t-surff: fully differential two-electron photoemission spectra, *New J. Phys.* **14**, 085008 (2012).
- [39] V. Mosert and D. Bauer, Photoelectron spectra with qprop and t-surff, *Comput. Phys. Commun.* **207**, 452 (2016).
- [40] D. E. Manolopoulos, Derivation and reflection properties of a transmission-free absorbing potential, *J. Chem. Phys.* **117**, 9552 (2002).
- [41] M. Edén and M. H. Levitt, Computation of orientational averages in solid-state nmr by gaussian spherical quadrature, *J. Magn. Reson.* **132**, 220 (1998).
- [42] N. Weinberg and K. Mislow, On chirality measures and chirality properties, *Can. J. Chem.* **78**, 41 (2000).
- [43] C. Lux, M. Wollenhaupt, C. Sarpe, and T. Baumert, Photoelectron circular dichroism of bicyclic ketones from multiphoton ionization with femtosecond laser pulses, *ChemPhysChem* **16**, 115 (2015).
- [44] R. Mehrem and A. Hohenegger, A generalization for the infinite integral over three spherical bessel functions, *J. Phys. A* **43**, 455204 (2010).